Heterogeneous Photocatalytic Oxidation of 1-Butene on SnO_2 and TiO_2 Films

Lixin Cao, Franz-Josef Spiess, Aimin Huang, and Steven L. Suib*

Department of Chemistry, U-60, University of Connecticut, Storrs, Connecticut 06269-4060

Timothy N. Obee, Steven O. Hay, and James D. Freihaut

United Technologies Research Center, 411 Silver Lane, East Hartford, Connecticut 06108

Received: September 24, 1998; In Final Form: January 12, 1999

Three types of films were prepared by a dip-coating process for the photocatalyzed decomposition of 1-butene in a gas−solid reaction. Under UV illumination (λ > 300 nm, 352 nm peak intensity), ultrasmall SnO_2 with a diameter of 5 nm exhibited initial photoactivity as high as 3 times that of P-25 TiO_2 (30 nm) in the absence of water vapor whereas SnO_2-1 (22 nm) did not show photoactivity. Quantum size effects were mainly responsible for the high photoactivity achieved by SnO_2. Inactivity of SnO_2-1 film was due to the absence of active hydroxyl groups on the catalyst surface and low surface areas. By investigation of the effects of humidity, water has two different functions: maintaining constant oxidation rates at low water levels by replenishing hydroxyl groups and decreasing the photoactivity at high water levels by competitive adsorption with butene on active sites. Compared with TiO_2, SnO_2 cannot withstand high humidity since it is very sensitive to water concentration. Hydroxyl groups on catalyst surfaces are the active centers for the reaction. The occurrence of obvious deactivation on SnO_2 films was due to the depletion of hydroxyl groups and the accumulation of carbonate species on particle surfaces, i.e., M−OCOOR species in place of M−OH. The kinetic data correlate with a Langmuir−Hinshelwood single-site model. XRD, UV−vis spectroscopy, and FTIR techniques were employed to characterize the particle size, band gaps, and surface properties of the catalysts.

Introduction

The elimination of trace-level organic contaminants in air has recently drawn much attention since this technology can be potentially applied for air purification in homes, office buildings, factories, cars, and spacecraft. Decontamination of toxic organic chemicals over semiconductor materials, illuminated with UV or visible light, is a promising technique for these applications. Of these semiconductors (e.g., TiO_2, ZnO, Fe_2O_3, CdS, ZnS, $SrTiO_3$, etc.),[1−4] much work has been devoted to Degussa P-25 TiO_2 because of its high photoactivity, excellent stability, and low cost. Furthermore, P-25 TiO_2 has been chosen as a standard photocatalyst for comparison of results between groups.[5] This commercially available TiO_2 is mostly anatase in crystalline form (anatase: rutile ratio, 70:30) and has a surface area of about 50 m^2/g, a primary particle size of 30 nm, and a band gap of 3.2 eV. Although many types of semiconductors, as well as TiO_2 modified with some dopants, have been extensively studied in gas−solid photocatalytic reactions, so far no significantly better materials than Degussa P-25 TiO_2 have been reported.

Recently, there has been a substantial body of work focused on the photochemical characteristics of ultrasmall particles (i.e., Q-sized particles).[6,7] The advantages of Q-sized particles over macroparticles relate to the following factors: (i) These small particles with diameters between 1 and 10 nm exhibit characteristics between molecular and bulk semiconductors. (ii) The blue shifts of the band gap in UV−vis adsorption for Q-sized particles enhance the redox potentials of the photogenerated electrons and holes. (iii) The high surface-area-to-volume ratios lead to improved effectiveness for surface-limited reactions. On the basis of these unusual properties of Q-sized semiconductors, limitations of poor photoefficiency for macroparticles may be overcome by the use of Q-sized semiconductor particles. Much work has been devoted to colloidal semiconductor photochemistry in this field.[8]

Some researchers have used thin nanocrystalline SnO_2 semiconductor particulate films as electrodes for electrochemical and photoelectrochemical reactions.[9] The spectral responses of SnO_2 and TiO_2 are quite similar as SnO_2 is an n-type semiconductor with a band gap of 3.8 eV. In this paper, Q-sized SnO_2 film was developed to compare with TiO_2 (P-25) and macrocrystalline SnO_2 under UV (352 nm) illumination for the oxidation of 1-butene. The initial activity of SnO_2 was 3 times higher than that of TiO_2 in the absence of water vapor, although deactivation was observed. The high activity of SnO_2 is mainly due to Q-size effects. Kinetically, a Langmuir−Hinshelwood single-site mechanism has been used to describe the reaction. The deactivation of SnO_2 was investigated using FTIR techniques.

Experimental Section

Apparatus. Experimental data were generated in a glass-plate photocatalytic reactor. A detailed description of the reactor and its operation is presented elsewhere.[10] The reactor was operated as a differential reactor using high flow rates (3.6 L/min) and low conversion of 1-butene. UV illumination was done with a pair of black-light lamps (λ > 300 nm, 352 nm peak intensity, SpectroLine XX-15A). The UV intensity at the catalyst surface was measured with a UVA power meter (Oriel UVA Goldilux) and was 0.63 mW/cm^2. Standard nitrogen passed through a water bubbler to obtain the desired water vapor level in the feed stream. An oxygen gas flow mixed with

* To whom correspondence should be addressed.

10.1021/jp983860z CCC: $18.00
Published on Web 03/26/1999

nitrogen and 1-butene produced the desired carrier gas mixture. GC (HP-5890 II) equipped with an FID detector and a RTX-1 column (RESTEK Corp.) was used to measure 1-butene concentrations. The concentrations of water were measured using a humidity and temperature transmitter (Vaisala) calibrated with a more accurate photoacoustic detector (Brüel & Kjær 1302). This operation was done at room temperature (22−25 °C) and approximately atmospheric pressure.

Materials. The films were deposited on microscope glass slides (7.5 cm × 1.8 cm) with surface areas of 13.5 cm^2 using a dip-coating process. SnO_2 colloidal suspensions (15 wt %) were obtained from Alfa Chemicals. The colloidal SnO_2 was heated at 100 °C for 6 h. After complete dehydration, chunks of SnO_2 were ground to fine powders. Since the dehydration of colloidal SnO_2 is irreversible, powdered SnO_2 suspended in distilled water (50 wt %) for making films was no longer colloidal. TiO_2 suspensions (15%) were prepared by adding Degussa P-25 TiO_2 into distilled water and stirring the suspension for 24 h. SnO_2-1 suspensions (50 wt %) in which the SnO_2 solid powder was obtained from the Coleman & Bell Co. were prepared with the same procedures as TiO_2. The films were prepared by dipping the glass slides separately in the suspensions several times until they were thick enough (approximately 2.0 mg/cm^2) to prevent UV light from penetrating the slides.

Characterization Methods. The XRD patterns were obtained using a Scintag model PDS-2000 diffractometer with a Cu Kα radiation source. The X-ray tube was operated at 45 kV and a current of 40 mA. Scherrer equation[11] was employed to compute the average particle size.

The UV−vis absorption of the films was measured with an HP 8452A spectrometer. In this study, the ultrathin films, which are much thinner than the films used in the photocatalytic reactions, were coated on quartz slides. Clean quartz was used as a reference background.

The diffuse-reflectance FTIR results were obtained on a Nicolet Magna-IR 750 spectrometer. The measured samples were scraped from the films before or after reaction.

BET surface areas were determined by nitrogen adsorption and desorption data acquired on an Omicron Omnisorp-100 CX analyzer.

Results

All tests in this study were performed at a 3.6 L/min volumetric flow rate. The effect of external mass transfer under such conditions can be neglected.[12] The data thus represent the intrinsic chemical kinetics of surface reactions, which is the rate-limiting step in the reaction.

To ensure differential conditions, the conversion of butene was controlled at low levels (around 10%) throughout the catalyst bed by changing the number of slides (i.e., the illuminated area). In this study, the intensity of UV light, determined by varying the distance between lamps and the catalyst surface, was maintained at a constant UV power flux of 0.63 mW/cm^2. Each slide has a surface area of 13.5 cm^2. The films deposited on the slides are opaque enough to prevent UV light from penetrating the slides. In a study of the oxidation of trichloroethylene, Jacoby et al.[13] suggest that the reaction rate increased with film loading up to a P-25 TiO_2 loading of 0.5 mg/cm^2 and additional film loading contributed nothing to photoefficiency. This conclusion was applied to our systems. The loadings of SnO_2, SnO_2-1, and TiO_2 are about 2.0 mg/cm^2 in this study. No conversion of 1-butene was observed after the UV lamps were switched off.

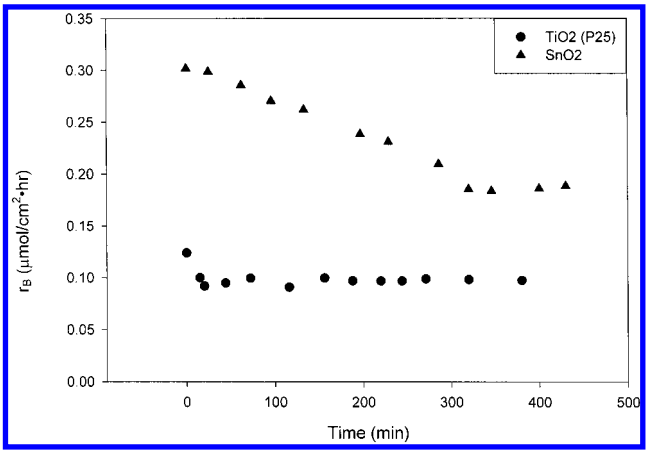

Figure 1. Dependence of oxidation rate on time in the absence of water vapor, I_0 = 0.63 mW/cm^2, flow rate = 3.6 L/min, C_{B0} = 2.75 ppm.

The experiments were conducted at room temperature (22−25 °C) and atmospheric pressure. Therefore, if the volumetric flow rate is 3.6 L/min and the area of each slide is 13.5 cm^2, the reaction rate can be directly computed according to the following equation

$$r_B = 0.654 x C_{B0}/N \quad (1)$$

where r_B (μmol/cm^2·h) is the 1-butene oxidation rate, x is the conversion of 1-butene, C_{B0} (ppm) is the butene inlet concentration, and N is the number of slides used for photocatalytic reaction.

Photocatalytic Activity. For comparison of photocatalytic activity, three different films were prepared using similar processes. Figure 1 shows the oxidation rate of butene as a function of time over different films. SnO_2-1 films (precursor is commercially available solid powder) have no photoactivity. In the present study, no moisture was introduced into the feed stream. The molar oxygen concentration was 10%. The 1-butene inlet concentration was 2.75 ppm. Our experimental data indicated that conversion of butene on SnO_2 at the beginning of the reaction was 17.3% using one slide with an area of 13.5 cm^2. However, under identical conditions, TiO_2 gave only 5.5% conversion of butene on each illuminated slide. In the initial stage, SnO_2 presented photoactivity as high as 3 times that of P-25 TiO_2, but obvious deactivation was observed on SnO_2 films, which lasted for 6 h until the oxidation rate reached a constant level (0.18 μmol/cm^2·h). The P-25 TiO_2 rapidly reached a constant oxidation rate after 0.5 h. We observed that the films turned pale yellow after reaction. The vent gases were cooled using dry ice in order to trap partially oxidized products. Only water was detected. We also attempted to use methanol to extract adsorbed compounds from the used films. Nothing was found, although FTIR results confirmed the presence of carbonyl groups as shown in the spectrum of Figure 7.

Effects of Humidity. To investigate the effects of humidity on the photocatalytic activity of SnO_2 and TiO_2 films, small amounts of water vapor (100 ppm) were first fed into the flowing stream. These experiments demonstrated that the oxidation rate on SnO_2 was very stable (0.16 μmol/cm^2·h) in the presence of trace amounts of water vapor in the feed stream (Figure 2). Although the reaction rate was stable, it was lower than that under dry conditions. Small amounts of water vapor do not affect the photoactivity of TiO_2 to a substantial degree since the oxidation rates in the presence and absence of trace moisture are similar. The finding that no deactivation occurs with trace

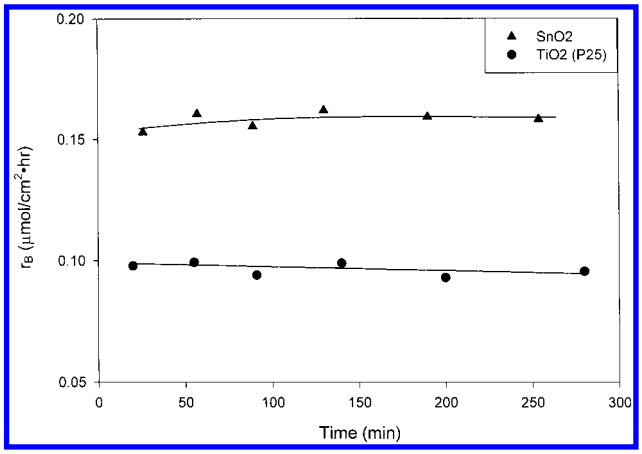

Figure 2. Comparison of oxidation rates of SnO_2 and TiO_2 films in the presence of trace feedwater, $I_0 = 0.63$ mW/cm^2, flow rate = 3.6 L/min, $C_w = 100$ ppm.

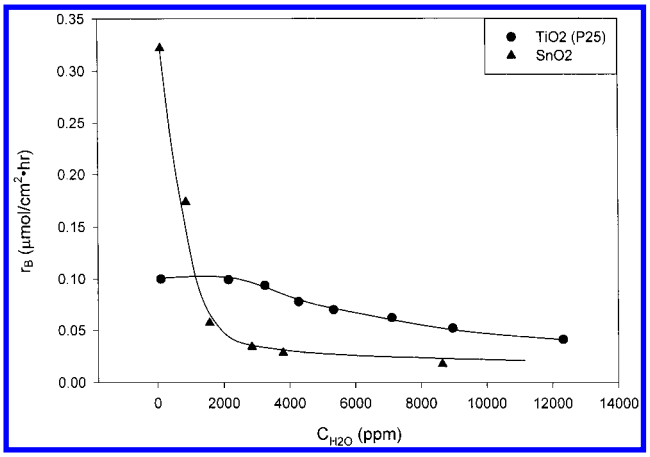

Figure 3. Oxidation rate of 1-butene vs water concentration in the gas phase, $I_0 = 0.63$ mW/cm^2, flow rate = 3.6 L/min, $C_{B0} = 2.75$ ppm.

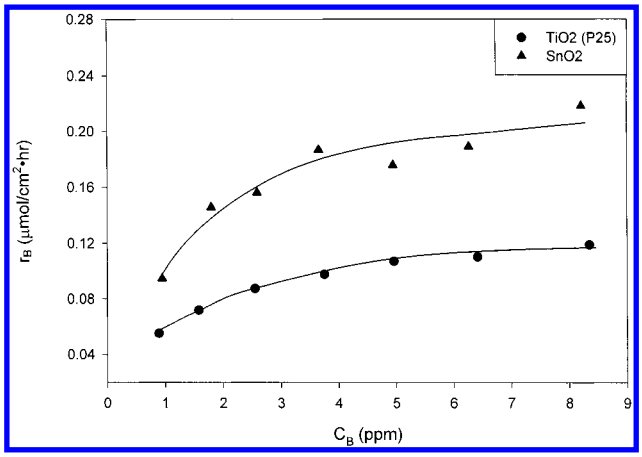

Figure 4. Oxidation rate vs 1-butene inlet concentration, $I_0 = 0.63$ mW/cm^2, flow rate = 3.6 L/min, $C_w = 100$ ppm.

amounts of water vapor is critical to our further studies, because stable photoactivity is a prerequisite for kinetic studies.

Further investigation of the effects of humidity on oxidation rate is illustrated in Figure 3. The oxidation rate on SnO_2 drops dramatically with increasing moisture in the feed steam. High photoactivity of SnO_2 is only apparent at low water vapor level (<1000 ppm), while very poor photoactivity is observed after the water concentration increases up to 2000 ppm. In contrast, TiO_2 films maintain a stable oxidation rate even though the water concentration varies from 0 to 3000 ppm. At high water

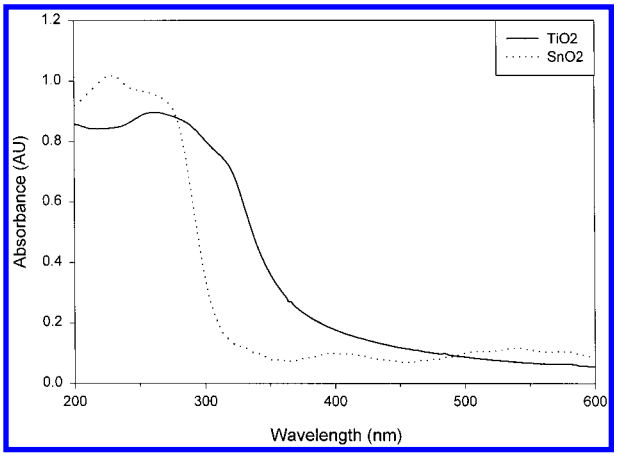

Figure 5. Absorption spectra of SnO_2 and TiO_2 ultrathin films.

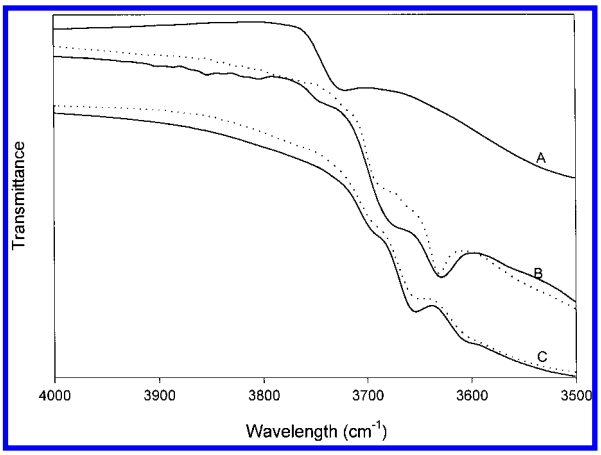

Figure 6. FTIR spectra of SnO_2-1 (A), TiO_2 (B), and SnO_2 (C) in the −OH stretching region: (—) before reaction, (···) after reaction.

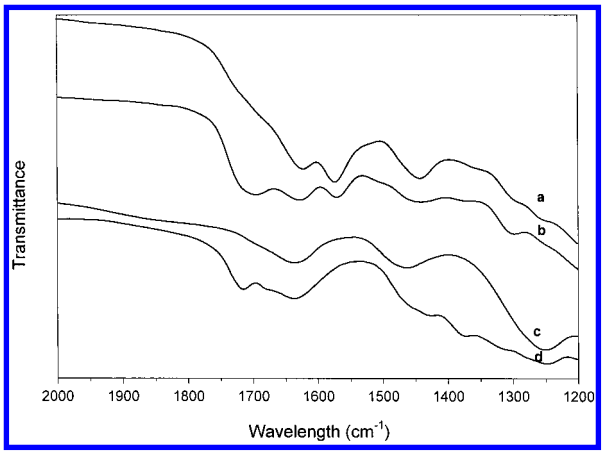

Figure 7. FTIR spectra of TiO_2 and SnO_2 before and after reaction in the C═O stretching region: (a) TiO_2 before reaction, (b) TiO_2 after reaction, (c) SnO_2 before reaction, (d) SnO_2 after reaction.

concentrations, the oxidation rate on TiO_2 decreases gradually and exceeds SnO_2. SnO_2 is much more sensitive to humidity than TiO_2. Compared to TiO_2, SnO_2 cannot tolerate high humidity. The loss in activity at high humidity on TiO_2 is supported by research of Ollis[12] and others.[14]

Effect of Butene Concentration. In this study, low levels of water (100 ppm) were chosen to maintain constant photocatalytic activity. The butene inlet concentrations varied from 1 to 9 ppm. Our experimental results showed that conversion of butene decreased with increasing butene concentration. However, the oxidation rate, determined by the combination of the conversion and the inlet concentration of butene (eq 1),

TABLE 1: Langmuir−Hinshelwood Correlation Coefficients

catalyst	k_0 (μmol/cm^2·h·ppm)	K_w ($\times 10^4$, ppm^{-1})	K_B (ppm^{-1})	no. of data points
SnO_2	0.33	74.9	1.36	6
TiO_2	0.12	4.58	0.85	7

TABLE 2: XRD Results and BET Surface Areas for Different Catalysts

catalyst	particle size (nm)	crystalline phases	surface area (m^2/g)
TiO_2	29	anatase + rutile	49.5
SnO_2	5	rutile	178.7
SnO_2−1	22	rutile	8.9

increases with butene concentration (Figure 4). Under these circumstances, SnO_2 films still exhibit higher activity than TiO_2 films as long as only trace water vapor is present in the feed stream. The changing magnitude of oxidation rate at low concentrations of butene is higher than at high concentrations. No deactivation on SnO_2 and TiO_2 films was observed within 3 h, even though the concentration of butene was as high as 8.5 ppm.

Kinetic Studies. The Langmuir−Hinshelwood (L−H) model has been extensively adopted to probe the surface reaction on a given photocatalyst in liquid-phase photocatalysis[3] and is also useful for gas-phase oxidation.[10,15] For most heterogeneous photocatalytic reactions, the L−H single-site mechanism is a good model for oxidation rate data. The simplified L−H mechanism is expressed by

$$r_B = k_0 C_B/(1 + K_B C_B + K_w C_w) \quad (2)$$

where k_0 is the overall specific reaction rate and K_B and K_w are the Langmuir adsorption equilibrium constants for butene and water, respectively. The oxygen concentrations between the inlet and outlet almost remained unchanged since its composition in the feed stream was approximately 10%, much higher than 1-butene whose inlet concentrations ranged from 1 to 9 ppm. Jacoby et al.[13] have found that the reaction rate for the oxidation of trichloroethylene is zero order with respect to oxygen if the oxygen concentration is higher than 1%. Thus, it is reasonable to assume that the reaction rate is independent of oxygen concentration in this case. The model is also based on the assumption that the possible reaction products (CO_2 or CO) do not influence the observed oxidation rates and that only adsorption of butene and water vapor is important. On the basis of the above assumptions, the L−H model can be tested by the closeness to linearity of plots of C_B/r_B versus C_B and C_w. The L−H rate coefficients for the correlation are given in Table 1. Figure 1 shows that the oxidation rates of 1-butene decrease linearly within 6 h in the absence of water vapor in the feed stream. The apparent kinetics of deactivation of SnO_2 are zero order according to Fogler's analysis of deactivation.[16]

Catalyst Characterization. To investigate the nature of the catalysts used in this study, XRD, BET, UV−vis spectroscopy, and FTIR techniques were used to characterize the particle sizes, surface areas, band gaps, and surface properties, respectively.

XRD patterns show that diffraction peaks of SnO_2 are much broader than those of TiO_2 and SnO_2-1. The Scherrer equation[11] was applied to approximately compute the average particle size. XRD results are listed in Table 2. The computed particle size of P-25 TiO_2 is very close to the value of 30 nm given in the literature.[3]

Results of BET surface areas are listed in Table 2. The surface area of P-25 TiO_2 is very close to 50 m^2/g given in the literature.[3] SnO_2 has a much higher surface area than TiO_2 and SnO_2-1. This could be due to the smaller particle size of SnO_2.

Figure 5 shows the UV−vis spectra of TiO_2 and SnO_2. The band gaps of SnO_2 and TiO_2 are 3.8 and 3.2 eV, respectively. The corresponding wavelengths are 327 and 386 nm. The onset of adsorption for both samples shown in Figure 5 closely matches the band gaps of SnO_2 and TiO_2. The UV absorption of TiO_2 is consistent with other results.[17] The emission of the black-light lamps used in our studies ranges from 300 to 400 nm. The maximum emission of the lamps is 352 nm, which is suitable for TiO_2. Owing to the difficulty in making ultrathin SnO_2-1 films, no UV−vis absorption spectrum is available for SnO_2-1.

Hydroxyl groups on the catalyst surface are believed to be active sites for the adsorption of reactants. FTIR spectra (Figure 6) show that hydroxyl groups exist on TiO_2 and SnO_2 in the region of 3600 to 3700 cm^{-1}. Some authors[18,19] observed two types of hydroxyl groups on TiO_2 surfaces. The one at higher frequencies corresponds to more basic hydroxyl groups, and the one at lower frequency corresponds to more acidic ones. In the present study, similar peaks for TiO_2 occur at 3629 and 3671 cm^{-1}. These bands are generally assigned to free hydroxyl groups in the case of metallic oxides. The typical hydroxyl group vibration on SnO_2 is found at 3658 cm^{-1}. There are two weak bands at 3618 and 3692 cm^{-1}, respectively. However, no such vibrational bands in this region are observed on the surface of SnO_2-1 (Figure 6 A). In contrast, a band at high wavelength (3721 cm^{-1}) is assigned to free hydroxyl groups on the surface of SnO_2-1. This type of hydroxyl group is very basic in comparison to hydroxyl groups on SnO_2. Such hydroxyl groups are not believed to be active sites according to our observations.

Figure 6 shows changes of the intensities of −OH infrared bands on catalyst surfaces before and after reaction. The vibrational intensity, which is supposed to be proportional to the number of hydroxyl groups under given conditions, declines on deactivated SnO_2. The decrease in intensities of −OH vibrations on TiO_2 after reaction can be seen in Figure 6B. These data suggest that some hydroxyl groups permanently disappear during the reaction. FTIR results are consistent with the argument that hydroxyl groups are the active sites. Partial deactivation on SnO_2 and TiO_2 is due to loss of hydroxyl groups.

Discussion

Q-Size Effects. Under UV illumination, a semiconductor particle absorbs light and generates delocalized electrons in the conduction band and delocalized holes in the valence band that are uniformly distributed throughout the particle. Within a few picoseconds after photon absorption, these free delocalized carriers migrate to the particle surface and get trapped at various surface sites or annihilate via electron−hole recombination. The initial stages concerning photocatalysis processes are described[1,12,20] below

$$TiO_2 + h\nu \rightarrow h^+ + e^- \quad (3)$$

$$h^+ + OH^- \rightarrow \bullet OH \quad (4)$$

$$Ti^{4+} + e^- \rightarrow Ti^{3+} \quad (5)$$

$$Ti^{3+} + O_{2ads} \rightarrow Ti^{4+} + O_{2ads}{}^- \quad (6)$$

$$\bullet OH + \text{pollutant} \rightarrow \text{oxidized pollutant} \quad (7)$$

$$\text{recombination: } h^+ + e^- \rightarrow \text{thermal heat or luminescence} \quad (8)$$

According to the above mechanism, the critical process for photocatalytic reactions is determined by the competition between charge transfer (steps 4 and 5) and recombination of electrons and holes (step 8). The reason most semiconductors exhibit poor photoefficiency is that the recombination process is much faster than the carrier trapping process. One possible way to overcome the drawback is to increase either the recombination lifetime or the carrier trapping process. Q-sized particles are potential candidates for enhancing photoefficiency. Semiconductor particles exhibiting quantum size effects are often referred to as Q-sized particles. These ultrasmall particles with diameters ranging from 1 to 10 nm possess unique properties which span the physical domain between molecular compounds and bulk materials.[6] Particles with diameters ≥ 15 nm apparently behave as bulk semiconductors.

In general, the ultrasmall particles only are stable in suspensions or as powder if these particles are trapped in various media, for instance, organic compounds or polymers. In the course of catalyst preparation in our study, the suspension was dried until solid chunks of SnO_2 were formed. During these processes, these ultrasmall particles might agglomerate because of the strong surface tension and plentiful defects on the surfaces. However, instead of close-packing, the particles just loosely stick together to form clusters. Therefore, the individual particle in a cluster still exhibits Q-size character. Some evidence for this assumption is that the surface area of SnO_2 is much higher than that of TiO_2 and SnO_2-1 (Table 2). According to this criterion, SnO_2 used in our experiments still has typical properties of Q-sized particles whereas TiO_2 and SnO_2-1 show bulk semiconductor properties (Table 1).

One of the important factors of Q-size effects is the high ratio of surface area to volume. The specific surface areas increase with decreasing particle size. High surface areas inevitably enhance the catalytic efficiency, especially for surface-limited reactions, like the reaction in this study. Therefore, high surface areas contribute to the high photoactivity of SnO_2. This is confirmed by the great variation in surface areas between SnO_2-1 and SnO_2.

In the present study, UV lamps with a peak intensity of 352 nm should be more suitable for TiO_2 films than SnO_2 films (Figure 5). Under identical operating conditions, however, SnO_2 exhibited much higher photoactivity than P-25 TiO_2 (Figure 1), which is considered to be an active photocatalyst in many studies.[3] An explanation for this observation is that the carrier trapping process occurs faster in Q-sized particles than in bulk materials by accelerating the migration of electrons and holes from inside the particles to the outer surface. The recombination process is overwhelmed by the carrier trapping process. This gives rise to high photoefficiency for Q-sized SnO_2 films in comparison with large particle materials.

Notwithstanding, the difference in band gaps between SnO_2 and TiO_2 is also responsible for the high photoactivity of SnO_2. The high-energy band gap of SnO_2 enhances the redox potential of the photogenerated electrons and holes, even though the light source matches the absorption bands of TiO_2.

In this paper, we are unable to measure the threshold wavelength of SnO_2-1 because of the difficulty in preparation of ultra-thin SnO_2-1 film. We thus have no reference to indicate the blue shift caused by "Q" particles. However, we prepared Q-sized TiO_2 catalysts and observed a blue shift in relation to P-25 TiO_2. We also made a series of TiO_2 catalysts with different surface areas (from 100 to 300 m^2/g). High surface area materials (>200 m^2/g) reversibly decreased the reactivity of TiO_2 films. Only TiO_2 films with moderate surface area (~ 150 m^2/g) exhibited high photoefficiency.

Effects of Humidity. Photocatalytic processes are complicated. These involve not only the absorption of light and the transfer of electrons and holes, but also the adsorption of reactants, surface reactions, and desorption of products. Steps 4 and 7 emphasize the role of hydroxyl groups during photoreaction. The importance of surface hydroxyl groups is related to two aspects: scavenging of holes and adsorption centers for reactants and intermediates. By investigating the adsorption of benzene and its derivatives on TiO_2 surfaces, Nagao and Suda[21] suggested that these molecules were adsorbed by formation of $Ti^{4+}\cdots\pi$ electron type complexes and by formation of $OH\cdots\pi$ electron type complexes on hydroxylated surfaces. In all likelihood, 1-butene adsorption is similar to benzene, i.e., $OH\cdot\cdot\cdot\pi$ electron type complex forms in our case. On the other hand, water can competitively adsorb on hydroxyl groups via hydrogen bonding,[23] which is expected to be stronger than the $OH\cdots\pi$ electron type complex. Water therefore plays two different roles in oxidation reactions: promotion of replenished hydroxyl groups and inhibition via competitive adsorption on hydroxyl groups with pollutants. These two functions of water are substantiated in our study.

In the absence of water in the feed stream, high photoactivity is realized due to maximum adsorption of reactants (Figure 1). At low water vapor levels, an adsorption−consumption balance of water is established on catalyst surfaces. Thus, a high and stable photocatalytic oxidation rate is achieved (Figure 2). At high water vapor levels, however, the pseudoequilibrium shifts toward water adsorption. The adsorption of reactants is strongly restricted, especially on the surface of SnO_2, due to the occupancy of active sites by water. Hence, photocatalytic activity decreases with increasing water concentration (Figure 3). The results obtained with the L−H correlation (Table 2) demonstrate the adsorption affinity of SnO_2 to water is much stronger than that of TiO_2 when comparing values of K_w. Compared to TiO_2, SnO_2 is very sensitive to water. SnO_2 has been extensively used as a moisture sensor for this very reason.[23]

Deactivation. The stability and photoactivity of catalysts are strongly influenced by the amounts and types of hydroxyl groups. Hydroxyl groups consumed in step 7 are generally replenished by dissociation of adsorbed water. Under dry conditions, depletion of hydroxyl groups cannot be replenished by water. The density of hydroxyl groups on the catalyst surface decreases as the reaction proceeds. This results in deactivation in time of TiO_2 and SnO_2. Dry conditions are not absolute since water can be formed in the reaction itself or delivered via carrier gases even at fairly low levels. Trace amounts of water balance the consumption−replenishment process of hydroxyl groups after a certain time of deactivation. Therefore, a constant oxidation rate is achieved on TiO_2 for 0.5 h and on SnO_2 for 6 h (Figure 1).

Photoactive hydroxyl groups fall into the range from 3600 to 3700 cm^{-1} in IR spectra (Figure 6). SnO_2-1 catalysts with one band at 3721 cm^{-1} have no photoactivity. A possible explanation is that OH groups are too strongly bound to be active sites. Thus, the SnO_2-1 surface is inert to 1-butene adsorption.

The role of hydroxyl groups as active centers is further verified by FTIR measurements (Figure 6). The declining intensities on deactivated SnO_2 and TiO_2 samples indicate that some hydroxyl groups are permanently consumed in the oxidation process. The loss in intensities of hydroxyl groups on SnO_2 is more remarkable than that on TiO_2. Correspondingly, SnO_2 exhibits obvious deactivation. In studies of oxidation of

trichloroethylene, TiO_2 loses photoactivity dramatically. After complete deactivation, no hydroxyl groups were observed on TiO_2 surfaces. The disappearance of hydroxyl groups is directly related to the loss of photoactivity in this case.

Photocatalytic deactivation in gas−solid reactions on TiO_2 has previously been reported by Cunningham[24] and Ollis.[25] Strongly chemisorbed intermediate species, for instance, carboxylic acids, are responsible for loss of photocatalytic activity. The adsorption of CO_2 on surfaces of TiO_2 can produce bicarbonate species.[18] Data of Figure 7 suggest that new species are formed on SnO_2 and TiO_2 surfaces after reaction. These distinct new peaks appear in the region of 1701 cm^{-1} on TiO_2 and 1719 cm^{-1} on SnO_2 and can be assigned to C═O vibrations of COO^- groups, which are accumulated on the catalyst surface in the process of butene oxidation. This observation is consistent with conclusions drawn by Cunningham[24] and Ollis.[25]

Combining the disappearance of hydroxyl groups with accumulation of carbonate groups on the catalyst surface, it is reasonable to infer that the deactivation in the oxidation of 1-butene proceeds as shown in the following step:

$$\text{M-OH} + \text{intermediates or products} \rightarrow \text{M}-\text{O}-\text{C}-\text{OR} \quad (9)$$

where R is hydrogen or alkyl groups.

L−H Model. As for kinetic studies, the following steps are consistent with the L−H single-site model:

$$\text{absorption of butene: } B + S \leftrightarrow B\bullet S \quad (10)$$

$$\text{surface reaction: } B\bullet S \rightarrow P + W\bullet S \quad (11)$$

$$\text{desorption of water: } W\bullet S \leftrightarrow W + S \quad (12)$$

If step 11 is considered to be rate-limiting, eq 2 can be readily derived from the above assumptions. Since oxygen is in great excess, it is excluded from this expression. The adsorption of CO_2 and other species are not taken into account, but CO_2 has been confirmed to be strongly adsorbed on the catalyst surface.[22]

Conclusions

The following conclusions were determined as a result of this research: (1) In the absence of water vapor in the flowing stream, SnO_2 with a particle size of 5 nm exhibits an initial photoactivity as high as 3 times that of P-25 TiO_2 for the photocatalytic oxidation of 1-butene whereas SnO_2-1 (22 nm) has no photoactivity. (2) Quantum size effects are mainly responsible for the high photoactivity achieved by Q-sized SnO_2. Relating the experimental results to FTIR spectra, it is found that the hydroxyl groups on solid surface are the active sites in the photocatalyzed oxidation. (3) Water has two functions in the photocatalysis process. Water maintains the constant oxidation rates at low levels and inhibits the adsorption of 1-butene at high levels. Compared to TiO_2, SnO_2 cannot afford high humidity since it is very sensitive to water concentration. (4) The kinetic studies indicate that this reaction follows the Langmuir−Hinshelwood model. (5) The formation of M−OCO-OR species on the catalyst surface results in deactivation in the oxidation of 1-butene. Deactivation is due to depletion of hydroxyl groups and accumulation of carbonate species on the catalyst surface. For SnO_2, the deactivation is zero order in the absence of feedwater.

Acknowledgment. We acknowledge United Technologies Research Center for support of this research.

References and Notes

(1) Hoffmann, M. R.; Martin, S. T.; Choi, W.; Bahnemann, D. W. *Chem. Rev.* **1995**, *95*, 69−96.
(2) Kamat, P. V. *Chem. Rev.* **1993**, *93*, 267−300.
(3) Fox, M. A.; Dulay, M. T. *Chem. Rev.* **1993**, *93*, 341−357.
(4) Mills, A.; and Le Hunte, S. *J. Photochem. Photobiol*. A: *Chem.* **1997**, *108*, 1−35.
(5) Matthews, R. W.; McEvoy, S. R. *J. Photochem. Photobiol*. A: Chem. **1992**, *66*, 355−366.
(6) Hoffman, A. J.; Yee, H.; Mills, G.; Hoffmann, M. R. *J. Phys. Chem*. **1992**, *96*, 5540−5546.
(7) Hoffman, A. J.; Mills, G.; Yee, H.; Hoffmann, M. R. *J. Phys. Chem.* **1992**, *96*, 5546−5552.
(8) Henglein, A. *Chem. Rev.* **1989**, *89*, 1861−1873.
(9) Vinodgopal, K.; Kamat, P. V. *Environ. Sci. Technol*. **1995**, *29*, 841845.
(10) Obee, T. N.; Hay, S. O. *Environ. Sci. Technol*. **1997**, *31*, 2034−2038.
(11) Azaroff, L. V. *Elements of X-ray Crystallography*; McGraw-Hill: New York, 1968; Chapter 20.
(12) Peral, J.; Ollis, D. F. *J. Catal*. **1992**, *136*, 554−565.
(13) Jacoby, W. A.; Blake, D. M.; Noble, R. D.; Koval, C. A. *J. Catal*. **1995**, *157*, 87−96.
(14) Phillips, L. A.; Raupp, G. B. *J. Mol. Catal*. **1992**, *77*, 297−311.
(15) Obee, T. N.; Brown, R. T. *Environ. Sci. Technol*. **1995**, *29*, 1223−1231.
(16) Fogler, H. S. *Elements of Chemical Reaction Engineering*, 2nd ed.; Prentice-Hall: Englewood Cliffs, NJ, 1992, Chapter 6.
(17) Paz, Y.; Luo, Z.; Rabenberg, L.; Heller, *A. J. Mater. Chem*. **1995**, *10*, 2842−2848.
(18) Primet, M.; Pichat, P.; Mathieu M.-V. *J. Phys. Chem.* **1971**, *75*, 1216−1220.
(19) Rob van Veen, J. A.; Veltmaat, F. T. G.; Jonkers, G. *J. Chem. Soc., Chem. Commun.* **1985**, *23*, 1656−1658.
(20) Harvey, P. R.; Rudham, R.; Ward, S. *J. Chem. Soc., Faraday Trans. 1* **1983**, *79*, 1381−1390.
(21) Nagao, M.; Suda, Y. *Langmuir* **1989**, *5*, 42−47.
(22) Raupp, G. B.; Dumesic, J. A. *J. Phys. Chem*. **1985**, *89*, 5240−5246.
(23) Andreev, S. K.; Popova, L. I.; Gueorquiev, V. K.; Stoyanov, N. D. *Sens. Actuators B* **1994**, *18*, 457−459.
(24) Cunningham, J.; Hodnett, B. K. *J. Chem. Soc., Far. Trans. 1* **1981**, *77*, 2777−2801.
(25) Sauer, M. L.; Ollis, D. F. *J. Catal*. **1996**, *163*, 215−217.